Journal of Materials Chemistry A

PAPER

View Article Online
View Journal | View Issue

Open Access Article. Published on 27 November 2015. Downloaded on 04/01/2016 06:14:04.
This article is licensed under a Creative Commons Attribution-NonCommercial 3.0 Unported Licence.

Cite this: J. Mater. Chem. A, 2016, 4, 632

# Nanoporous networks as effective stabilisation matrices for nanoscale zero-valent iron and groundwater pollutant removal†

P. D. Mines,[ab] J. Byun,[b] Y. Hwang,[ac] H. A. Patel,[b] H. R. Andersen[a] and C. T. Yavuz*[b]

Received 5th July 2015
Accepted 25th November 2015

DOI: 10.1039/c5ta05025a

www.rsc.org/MaterialsA

Nanoscale zero-valent iron (nZVI), with its reductive potentials and wide availability, offers degradative remediation of environmental contaminants. Rapid aggregation and deactivation hinder its application in real-life conditions. Here, we show that by caging nZVI into the micropores of porous networks, in particular Covalent Organic Polymers (COPs), we dramatically improved its stability and adsorption capacity, while still maintaining its reactivity. We probed the nZVI activity by monitoring azo bond reduction and Fenton type degradation of the naphthol blue black azo dye. We found that depending on the wettability of the host COP, the adsorption kinetics and dye degradation capacities changed. The hierarchical porous network of the COP structures enhanced the transport by temporarily holding azo dyes giving enough time and contact for the nZVI to act to break them. nZVI was also found to be more protected from the oxidative conditions since access is gated by the pore openings of COPs.

## Introduction

Current treatment practices for groundwater contamination, in particular hard to degrade contaminants like halogenated organics and azo dyes, have seen the application of zero-valent iron (ZVI) emerge as one of the most discussed and researched reactive materials. These materials are often in the form of *in situ* permeable reactive barriers, while applied extensively in *ex situ* (*i.e.* pump-and-treat) methods as well.[1] Globally, the use of ZVI has quickly gained traction because iron is ubiquitous in the earth's crust, cheap to manufacture, environmentally safe, and an effective reductant ($E^0 = -0.44$ V). Synthesizing ZVI on the nanoscale has been proven to dramatically increase the reactive capability of the iron particles due to the increase in the reactive surface area, increasing from 0.9 $m^2\ g^{-1}$ in commercially available micron-scale Fe-powder to 33.5 $m^2\ g^{-1}$ in nano-sized zero-valent iron (nZVI).[2] Over the years, nZVI has demonstrated the ability to be an effective degrading agent of a wide variety of pollutants, including antibiotics, azo dyes, chlorinated solvents, chlorinated pesticides, organophosphates, nitroamines, nitroaromatics, *p*-chlorophenol, polychlorinated biphenyls, inorganic ions, alkaline earth, transition, and post-transition metals, metalloids, and actinides.[3] In this study, our focus was dedicated towards azo dyes, which are the most widely used dyes in textile industries; and, because the destruction of the azo (N=N) bond by nZVI has been well documented over a range of various azo dyes.[4] Azo bond destruction allows for dye decolourization, making the reaction easy to identify and monitor in a standard laboratory. In this light, targeting the treatment of azo dyes with a stabilised nZVI calls for a simple indicator test of the particles' effectiveness for the abiotic reduction of both azo bonds and various other chemical bonds that ZVI is capable of reducing.[5]

Despite the superior decontamination properties, nZVI by itself is not a suitable material for practical water contaminant treatment in real-world applications. Bare nZVI particles have very limited transportability and flow in a porous medium, such as a subsurface contaminant plume, and exhibit a higher sticking coefficient, resulting in aggregated larger particles with substantially reduced reactivity.[6,7] The driving force behind the aggregation of nZVI particles comes from van der Waals and magnetic attraction forces.[6,8] In order to combat these inherent attractive forces of the nZVI particles and allow nZVI to be commercially used on a much larger scale, the idea of adding a stabilising agent has been identified in order to alter the surface characteristics of nZVI. Previously utilized stabilising agents include a variety of organic and inorganic species, including anionic surfactants, carbon particles, silica, clay, poly-acrylic acid, guar gum, xanthan gum, starch, carboxy-methyl cellulose, various polyelectrolytes, biopolymers,[9] and most recently a synthetic organoclay.[10] Despite a high volume of research dedicated to nZVI and its further applications, the challenge to develop a new synthetic method for generating

[a]Department of Environmental Engineering, Technical University of Denmark, Miljøvej, B113, DK-2800 Kongens Lyngby, Denmark
[b]Graduate School of EEWS, Korea Advanced Institute of Science and Technology, 291 Daehak-ro, Yuseong-Gu, Daejeon 34141, Republic of Korea. E-mail: yavuz@kaist.ac.kr
[c]Department of Environmental Engineering, Seoul National University of Science and Technology, 232 Gongneung-ro, Nowon-gu, Seoul 01811, Republic of Korea

† Electronic supplementary information (ESI) available. See DOI: 10.1039/c5ta05025a


This journal is © The Royal Society of Chemistry 2016

Open Access Article. Published on 27 November 2015. Downloaded on 04/01/2016 06:14:04.
This article is licensed under a Creative Commons Attribution-NonCommercial 3.0 Unported Licence.

stable and dispersive nZVI particles, without compromising their reactivity and the surface area in the presence of stabilising agents remains.

The past decade has seen the development of various porous organic materials targeting a plethora of applications, most often in the capture of carbon dioxide gas, such as those termed Covalent Organic Frameworks (COFs),[11] with certain studies reporting very promising results in this field.[12] However, these COFs have failed to reach the theoretical predictions for carbon dioxide capture capabilities[13] and have also proven, in many cases, to be unstable in water;[14,15] unless, for instance, the pores can be alkylated and hydrolysis can be prevented.[16] This lack of stability in water creates a major concern when dealing with environmental applications of organic polymers, in particular, when treating contaminated water sources. A particular type of porous network polymers, namely Covalent Organic Polymers (COPs), have received significant interest, particularly in environmental applications such as gas capture,[17–19] and water purification.[20] The main advantage of nanoporous COPs is their synthetic diversity in which various building blocks are employed to construct a rigid and stable porous polymer network with high surface area. Recently, it has been reported that COPs could be utilized as a porous support to generate palladium nanoparticles,[21] these composites of COPs and palladium nanoparticles exhibited excellent and stable performance as a heterogeneous catalyst for the carbon monoxide oxidation reaction. High surface area and functionality of the COPs enhance mass transfer for the adsorption of carbon monoxide molecules, and further stabilise the palladium nanoparticles without hindering the overall reactivity and surface area.

Herein, we introduce COPs as a new type of support material to stabilise nZVI particles. Rather than typical methods employed for stabilising nZVI that utilize a chemical coating technique, COPs present a highly porous polymeric network capable of physically caging nZVI within its matrix. This ability to trap nZVI stems from the amorphous web of interwoven polymer chains, anywhere from 10–50 nm in thickness, inherent in the polymer construction. Five different COPs having different surface areas and functionalities (amine, imine, thiol and ester) are employed to immobilize nZVI, where $Fe^{3+}$ ions in aqueous solution were adsorbed into the pores of COPs and simply converted into $Fe^0$ by *in situ* chemical reduction using sodium borohydride ($NaBH_4$). Hybrid composites exhibit a relatively high surface area compared to other solid supports reported in the literature,[8,22] showing good distribution of nZVI with good stability. Furthermore, the large granule of the composites is easily separated from the aqueous solution by simple filtration, which both prevents secondary water contamination and improves recyclability of the composites. The composites with nZVI and COP vary in their morphology, surface area, and wettability, and we compare the effect of the difference in physicochemical properties of the composites by analysing both the stability of composites in water, as well as azo dye removal efficiency. We believe that the proposed composites with different characteristics would offer ideas to understand key parameters for producing a stable and active nZVI for real field water treatment in both *in situ* and *ex situ* operations.

## Materials and methods

### Chemicals

All chemicals were used as obtained from the supplier; except for the organic solvents used in COP synthesis, the syntheses of which required that the solvents be made anhydrous *via* a solvent purification system. Complete details can be found in the ESI, section S1.†

### Synthesis of covalent organic polymer networks

In order to maintain nomenclature uniformity among various publications, COPs are numbered using an internal ordering system (visit http://PorousPolymers.com for a complete list). And, to better understand the polymeric structure of each COP, a table (Table 1) has been provided to outline the polymer structure of each COP used. Synthesis of COP-1 was performed following previously developed methods.[17] Synthesis of COP-6 was performed following previously developed methods.[18] Synthesis of COP-19 was performed following previously developed methods.[23] Syntheses of COPs 60 and 61 were performed similarly to that of COP-1, in that 2,2′,4,4′-tetrahydroxybenzophenone (COP-60) and 1,1,1-tris(4-hydroxyphenyl)-ethane (COP-61) monomers were added to benzene tricarbonyl trichloride before brought to reflux for 24 hours (COP-60) and 14 hours (COP-61), followed by purification by repetitive washing with selected solvents. ESI, section S2,† has in-depth details on the COP chemical compositions and synthesis methods of COPs 60 and 61.

Table 1 Chemical structure of each network used in this study

| Network | Structure |
|---|---|
| COP-1 | 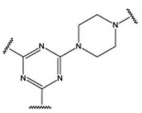 |
| COP-6 | 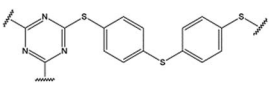 |
| COP-19 | 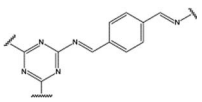 |
| COP-60 | 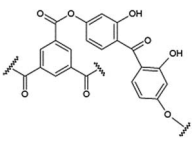 |
| COP-61 | 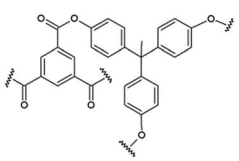 |

Open Access Article. Published on 27 November 2015. Downloaded on 04/01/2016 06:14:04.
This article is licensed under a Creative Commons Attribution-NonCommercial 3.0 Unported Licence.

### COP/nZVI composite synthesis

The procedure for the synthesis of the various COP/nZVI composite materials was derived from a method developed for immobilization of nZVI with alginate beads.[24] A solution containing 2.0% (w/v) COP/solvent, the solvent being water or *N*,*N*-dimethylformamide (DMF), and 0.05 M of $FeCl_3$ was mixed for 24 hours, in order to ensure full diffusion of $Fe^{3+}$ into the porous polymer matrix (*e.g.* 0.4 g of COP, 0.163 g of $FeCl_3$, and 20 mL of deionized water). This solution was then filtered under vacuum through a 0.45 μm glass-fiber filter until dry. The dried product was then re-solubilized with the solvent (water or DMF) and sonicated, to ensure complete dissolution. Conversion of the $Fe^{3+}$ to $Fe^0$ was performed by adding a 0.3 M solution of $NaBH_4$ in deionized water dropwise to an equal volume of the filtered and re-solubilized COP/$Fe^{3+}$ product, and mixed for 30 minutes under $N_2$-atmospheric conditions (*e.g.* 0.113 g of $NaBH_4$ in 10 mL deionized water was added to recovered COP/$Fe^{3+}$ mixed in 10 mL deionized water); this amount of $NaBH_4$ ensured that there was at least three times the amount of $NaBH_4$ for every $Fe^{3+}$. Following reduction, the solution was centrifuged and washed with ethanol three times, then dried for 12 hours in a vacuum environment at 120 °C. As for the control experiments, pure nZVI was prepared in the same manner, except for the absence of COP for immobilization.

### Physical characterisation

Fourier transform infrared (FTIR) spectroscopy was used to determine the functional groups of the individual COPs, spectra were recorded on KBr pellets using a Perkin-Elmer FT-IR spectrometer (Waltham, MA, USA). Morphological observation of the COP/nZVI composites was performed using a field emission transmission electron microscope (FE-TEM, Tecnai G2 F30 S-Twin model, FEI, The Netherlands). Preparation of the samples was done by solubilizing 5 mg of dried composite powder with 2 mL of ethanol, sonicating to ensure total dissolution, and placing three droplets of the said solution onto a carbon-coated copper mesh grid (300-mesh, FCF300-Cu Formvar Carbon Film, Electron Microscopy Sciences, Hatfield, PA, USA). The solution was allowed to dry on the Cu-grid for 30 minutes, and then subsequently analysed using FE-TEM. The total iron contained in each composite, including both impregnated iron within the polymer matrix and bound iron attached to the outside of the polymer matrix, was measured using inductively coupled plasma – mass spectrometry (ICP-MS, 7700 Series, Agilent Technologies, Santa Clara, CA, USA). Samples were prepared by digesting a solution of 2 mg of the composite and 1 mL of $HNO_3$ (60%) for approximately one hour (or until the sample was completely dissolved) at 80 °C, then filtering the digested solution through a 0.45 μm polytetrafluoroethylene (PTFE) membrane and diluted with deionized water.[25] Crystalline structures of the COP/nZVI composites were analysed using X-ray diffraction (D/Max-2500 model, Rigaku, Japan). Samples were scanned over a $2\theta$ range of 5–80° at a scan speed of 2° per minute. Analysis of the samples was performed in a vacuum-controlled environment. The total Brunauer–Emmett–Teller (BET) surface area and pore volume of each polymer and composite were measured using a Physisorption Analyzer (ASAP 2020, Micromeritics, Norcross, Georgia, USA). Prior to analysis, samples were degassed for 5 hours at 150 °C.

### Particle stability – sedimentation analysis

Stability of COP/nZVI composites was evaluated *via* sedimentation kinetics, using a Hach UV-Vis Spectrophotometer (DR 5000, Loveland, CO, USA). It was determined that the absorbance of metal nanoparticles in suspension is directly related to the particle size.[26] As all samples were prepared in the same manner, it was determined that the sedimentation rate was independent of solution viscosity. Freshly prepared samples were mixed with deionized water at a concentration of $550 \pm 20$ mg $L^{-1}$, sonicated, and transferred to a 1 cm plastic cuvette. Absorbance spectra of the samples were measured over a 60-minute period, at 508 nm, in order to obtain sedimentation curves, which were then interpreted using the following equation.[6]

$$A_t = A_0 \times e^{-t/\tau}$$

Where $A_t$ is the absorbance of the sedimenting solution at time $t$, $A_0$ is the initial absorbance, and $\tau$ is the characteristic time of sedimentation for the particles in solution.

### Particle reactivity – dye decolourization

The reactivity of the composite particles was determined by their ability to decolourize a solution of the azo dye, naphthol blue black. Previous work has proved the ability of granular $Fe^0$ to decolourize a variety of azo dyes,[5] and naphthol blue black was chosen in particular, due to its higher peak absorbance wavelength ($\lambda_{max} = 618$ nm), in order to minimize any absorbance interference from $Fe^{2+}$ or $Fe^{3+}$ ions that may form in solution during the test. All dye decolourization experiments used a solution of 10 mM HEPES buffer and 60 μM naphthol blue black in deionized water. This particular condition set with an organic buffer (HEPES) at 10 mM and pH = 7 had already been predetermined in a previous study[27] of $Fe^0$ in water to degrade contaminants as the optimal condition. The composite material was added to the dye solution at a concentration of 1.5 g $L^{-1}$ (Fe content of ~0.15 g $L^{-1}$), sonicated, and placed on a rotating mixer, then the samples were measured over a 30-minute period, in a wavelength range of 300–800 nm, in order to obtain a peak diminishing/decolourization curve from the spectra; similar to azo dye decolourization by $Fe^0$ methods reported previously.[28,29] All decolourization experiments were performed using deionized water under oxic conditions, to not only simulate real application, but also, as it has been previously determined that azo dyes are more effectively degraded by ZVI under oxic conditions.[30] Degradation products, specifically aniline, from the dye decolourization was measured using high performance liquid chromatography (HPLC, Agilent Technologies, 1100 Series, 1260 Infinity Degasser, Waldbronn, Germany; Sigma-Aldrich, Supelco Analytical Discovery® C18 column, 5 μm, 15 cm × 4.6 mm, Bellefonte, Pennsylvania, USA); using an eluent of methanol and 5 mM potassium dihydrogen phosphate.[31]

 This journal is © The Royal Society of Chemistry 2016

Open Access Article. Published on 27 November 2015. Downloaded on 04/01/2016 06:14:04.
This article is licensed under a Creative Commons Attribution-NonCommercial 3.0 Unported Licence.

# Results

### Properties of covalent organic polymers

Following the synthesis of each COP and before utilizing each COP, FTIR analysis was run on the polymers to confirm that the synthesis was a success and that the desired bonds had formed and certain functional groups were present (see ESI, section S3† for full analysis and FTIR scans). BET surface areas of each of the polymers varied substantially, from as low as 8.8 $m^2\ g^{-1}$ in COP-61, to as high as 600 $m^2\ g^{-1}$ in COP-19; BET results for all the polymers and composites used are detailed in Fig. 1(A).

### Properties of COP/nZVI composites

Morphologies varied between the various COP/nZVI composites, exhibiting globular cluster-like formations to thin sheath-like shapes. Although the exact shape and morphology are not necessarily important, being that the COPs are, by nature, amorphous; TEM images confirm that the particles are nano-sized, Fig. 2. Furthermore, when compared to similar TEM images of the COP by itself, to those already published of COP-1,[17] the composites display darker inner cores, evidencing that there is iron embedded within the COP matrix. In all cases, the cores of the matrix appear to have dark iron formations, where the iron has been trapped. Additionally, the reduction in the BET surface area of each composite confirms that there is nZVI being trapped and loaded into the pores of the polymer; which correlates similarly with a previous study that entrapped nZVI into the pores of activated carbon.[32] Also, it was found that the average pore size increased slightly with nZVI impregnation. This is mainly due to the presence of free-standing ZVI nanoparticles formed near and around the COPs, making additional pores by self-stacking of nanoparticles themselves.[33]

ICP-MS analysis of the composites revealed that iron had indeed been impregnated into the COP matrix. For the most part, the composites contained roughly 10% iron, by mass. Composites of COPs 1, 6, 19, 60, and 61 contained 9.1, 8.3, 9.2, 16.3, and 9.9% iron, respectively; outlined in Fig. 1(B). This is slightly higher than the observed values of 7.4% iron and 8.2% iron, when immobilizing nZVI onto alginate beads[24] and activated carbon,[32] respectively, indicating that the porous nature of COPs are better suited than both alginate and activated carbon for the impregnation of iron. In every case, the BET surface area of each of the composite dropped, with respect to the bare polymer used for that synthesis, due to both the filling and blocking of the micropores by nZVI. The comparison of which is outlined in Fig. 1(A).

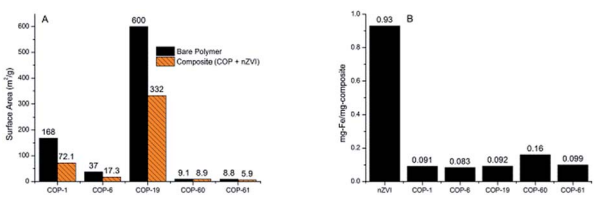


Fig. 1 BET surface area comparison of the bare polymer network *vs.* the COP/nZVI composite (A); and, the total iron content contained in each composite (B).

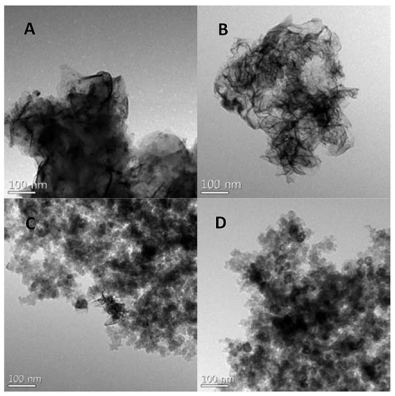


Fig. 2 TEM images demonstrating the composite morphology of COP-1 (A); COP-6 (B); COP-19 (C); and COP-60 (D).

When COPs are analysed with XRD, their amorphous non-crystalline structure yields no peak pattern, and therefore that data is not presented here. However, this means that any peak found in the composite scans is directly related to the iron impregnation; subsequently, the XRD analysis revealed that iron contained in the composites did reveal a $Fe^0$ peak. The characteristic peak of $Fe^0$ at 44.9° 2$\theta$ was clearly visible in the scans of each composite, except for the COP-6 composite, which did not exhibit any discernible peak pattern. Other than the composite of COP-6, the remaining XRD scans all produced a group of similar peak patterns. Although a definitive peak pattern could not be isolated for any one particular compound, various iron-based peaks do occur; in particular, bernalite ($Fe^{3+}(OH)_3$), maghemite ($Fe_2O_3$), lawrencite ($FeCl_2$), and magnetite ($Fe^{2+}Fe_2{}^{3+}O_4$), as is plotted in Fig. 3 for composites of COP-1 (A) and COP-19 (B). Although the $Fe^0$ peak appears small compared to the other peaks in the XRD patterns, it should be noted that the peak's intensity is still quite high compared to that of pure nZVI. For example, the $Fe^0$ peak in COP-1 is still 52% intensity of the pure nZVI peak and the $Fe^0$ peak in COP-19 is 79% intensity of the pure nZVI peak. As for the other peaks, $Fe_2O_3$ and $Fe_3O_4$ are easily produced during the air oxidation of iron.

The bernalite can be explained by the elemental iron reacting with water and dissolved oxygen once the $NaBH_4$ is consumed, see below the reaction scheme.

$$4Fe + 3O_2 + 6H_2O \rightarrow 4Fe^{3+} + 12OH^- \rightarrow 4Fe(OH)_3$$

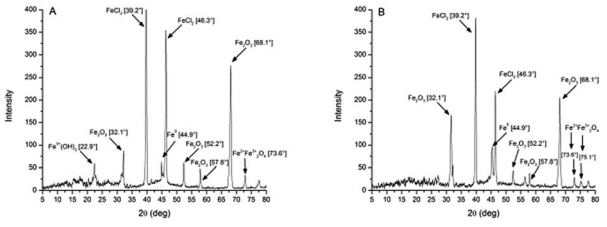


Fig. 3 XRD spectra patterns of composites of COP-1 (A) and COP-19 (B). Clearly visible is the $Fe^0$ peak at 44.9° 2$\theta$, indicating the presence of ZVI contained within the composite matrices.

Open Access Article. Published on 27 November 2015. Downloaded on 04/01/2016 06:14:04.
This article is licensed under a Creative Commons Attribution-NonCommercial 3.0 Unported Licence.

The lawrencite can be explained by the reaction of elemental iron with excess ferric chloride still in solution during the $NaBH_4$ reduction process, see below the reaction scheme.

$$Fe + 2FeCl_3 \rightarrow 3FeCl_2$$

And also as the product of anaerobic corrosion of iron in water followed by the precipitation of $FeCl_2$, see below the reaction scheme.

$$Fe + 2H_2O \rightarrow Fe^{2+} + H_2 + OH^-$$

$$Fe^{2+} + 2Cl^- \rightarrow FeCl_2$$

Therefore, the appearance of the various other peaks in the XRD spectra can be attributed to the inherently imperfect reduction process of $Fe^{3+}$ and potential oxidation during the sample preparation for XRD. XRD spectra patterns for the remaining composites, as well as for pure nZVI, are presented in the ESI, section S4.†

### Effect of COP on nZVI stability

The first and foremost requirement for making nZVI an applicable treatment technology is to make the nZVI itself stable in an aqueous environment. Therefore, for COPs to be an effective support material, it must be established that these COPs are both immune to the phenomenon of hydrolysis, as well as to establish that the composites are capable of maintaining suspension while in aqueous solution. The first parameter has already been proven, COP-1 for example, has been shown to remain stable in boiling water for weeks at a time.[17] Measuring the rate at which the composites aggregate and sediment out of solution can determine the second parameter, how effective the COPs are as a stabilising agent for nZVI, preventing iron aggregation and loss of reactivity. To illustrate this, Fig. 4(A) plots the relative absorbance of each composite suspended in deionized water, as well as pure nZVI, relative to the initial absorbance over a period of one hour; included in the plot are the calculated sedimentation curves, conducted as per the aforementioned method for particle stability.[6] Pure nZVI particles show very poor stability in deionized water, as expected, sedimenting out over 80% of its total mass, with nearly all of it settling out very quickly, within the first 15 minutes. COPs 1, 6, and 61 show improved stability compared to nZVI, sedimenting out 64, 64, and 59%, respectively; while also showing a much slower and linear sedimentation profile over the course of 60 minutes. COP-61 had even greater stability, sedimenting out only 39%. And, COP-19 exhibited highly stable sedimentation properties, after 60 minutes, only 3.9% of the initial absorbance had decreased. However, every one of these composites vastly outperforms certain previous attempts at a stabilised nZVI. For example, a study analyzed a surfactant modified nZVI from the NANOIRON® Company (Rajhrad, Czech Republic) at a concentration of 300 mg $L^{-1}$, compared to 550 mg $L^{-1}$ in this study, and found that over 80% of the particles settled out after a period of only 30 minutes.[34] At the equivalent point in time for this study, at nearly double the concentration, composites of COPs 1, 6, 19, 60, and 61 settled out 47, 49, 2.5, 32, and 50%, respectively. These percentage numbers can easily be put into perspective using the equation from Phenrat *et al.* (2006) to calculate the characteristic time, $\tau$, which can also be interpreted as a sedimentation "half-life" that determines how long it will take for particles to fall out of solution.[6] Characteristic times for bare nZVI and the composites of COPs 1, 6, 19, 60, and 61 are 14, 52, 49, 1340, 93, and 52 minutes, respectively; meaning that there is an increase in stability for each of the composites with respect to nZVI, and a very substantial increase for COP-19, proving the effectiveness of COPs as stabilising agents for nZVI. Although, the composites of COPs 1, 6, 60, and 61 have only similar or mildly better characteristic times as various other studies stabilising nZVI,[35–37] the composite with COP-19 has proven to be drastically better at stabilising nZVI by over a whole order of magnitude greater.

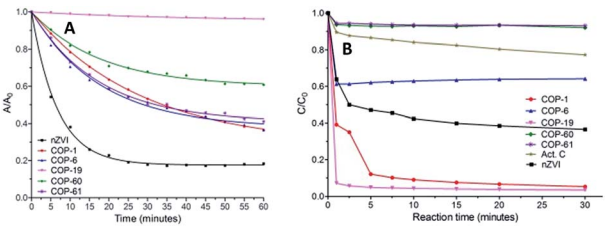


Fig. 4 Sedimentation profiles of nZVI and COP/nZVI composites, measured by the absorbance at 508 nm, in terms of absorbance relative to the initial absorbance, monitored over time (A); naphthol blue black decolourization over time by the composites, bare nZVI, and activated carbon (B).

### Effect of COP/nZVI composites on azo dye removal

There was a wide range of results in the ability of the composites to effectively decolourize the azo dye solution, which has been summarized in Fig. 4(B), plotting the absorbances (at the $\lambda_{max}$ = 618 nm) of the naphthol blue black solution when mixed with each composite, as well as activated carbon and bare nZVI, over time. After a 30 minute reaction period, the spectra of COPs 60 and 61 displayed almost no change, only producing a minimal reduction in the total absorbance, 8.0 and 7.0%, respectively. Fairing slightly better, COP-6 was capable of decolourizing the solution by 36%; however the shape of the curve remained exactly the same, indicating only adsorption and no degradation. Ultimately, COPs 1 and 19 achieved excellent dye removal rates, producing 95 and 97% absorbance decreases, respectively, Fig. 5(A and B). The remaining UV-Vis spectra for the composites not detailed in Fig. 5 can be found in the ESI, section S5.† In order to compare how the composites fared against the standard adsorbent for the water treatment industry, activated carbon was also tested for decolourization of naphthol blue black. It was observed that activated carbon is a very poor agent for decolourization of naphthol blue black; the

 This journal is © The Royal Society of Chemistry 2016

Open Access Article. Published on 27 November 2015. Downloaded on 04/01/2016 06:14:04.
This article is licensed under a Creative Commons Attribution-NonCommercial 3.0 Unported Licence.

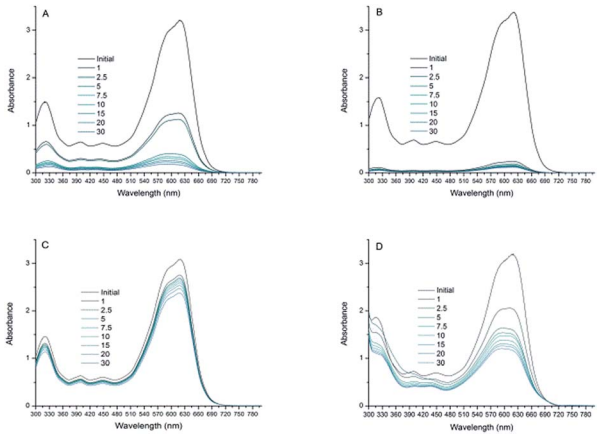


Fig. 5 UV-Vis absorbances for COP-1 (A); COP-19 (B); activated carbon (C); and bare nZVI (D).

spectra, Fig. 5(C), displayed a slow and minimal shift downwards and absolutely no change in the shape, indicating no degradation, only slow adsorption to the active binding sites of the carbon. COPs 60 and 61 proved to be very ineffective, much less so than activated carbon; however, it should be noted that COPs 1, 6, and 19 all fared better than that of activated carbon.

It was observed, over time, in the spectra for COPs 1 and 19, that the peak absorbance ($\lambda_{max}$ = 618 nm), indicative of azo bonds, gradually shifted to 588 nm and that the spectra peak at 310 nm, indicative of naphthalene groups, was also reduced. This pattern in the spectra observed in COP-1 and, to a lesser extent, in COP-19, Fig. 5(A and B), correlated to previous observations when degrading naphthol blue black with $Fe^0$, where it was concluded that these two phenomena in the peaks at 618 nm and 310 nm, degraded the azo bonds *via* reduction and oxidized the naphthalene groups *via* the Fenton reaction, respectively.[38] In order to confirm the results of Chang *et al.* (2009), when bare nZVI in this study was tested, the peaks at 618 and 310 nm behaved in the same manner, Fig. 5(D). Furthermore, this spectral pattern in naphthol blue black, and primarily the peak absorbance shift to lower wavelengths, was previously observed when reducing naphthol blue black by hydrogenation in the presence of platinum black,[39] and again when performing visible light induced degradation of naphthol blue black on $TiO_2$ nanoparticles.[40] Due to the pattern similarity of the observed spectra and experimental conditions, it can be assumed that the composite of COP-1 also degrades naphthol blue black in the same manner. It is also believed that the composite of COP-19 behaves similarly; however, the powerful adsorptive properties of COP-19 make determination of naphthol blue black degradation harder to distinguish. If in fact degradation of the dye is taking place, certain degradation products would be likely to appear in the dye solution; two primary coloured degradation products have been identified, Chromotrope 2B and Chromotrope 2R, with peak absorbances of 514 nm and 512 nm, respectively.[40] However, the coloured nature of these compounds could lead to analytical uncertainty when using UV-Vis spectroscopy. So, it was decided to focus on the smaller degradation products, in particular, aniline, which can be quantitatively identified *via* HPLC. Another study focused on the degradation of naphthol blue black, utilizing photocatalysis, has proposed the mechanism (Scheme 1) for how this aniline production would be expected to take place.[31]

In order to confirm what the spectra indicated, that there was degradation taking place, samples from the dye reaction with the most promising candidate, the COP-1 composite, were tested for aniline production. Analysis with HPLC produced positive results, and did confirm the presence of aniline after the reaction began, however, only a minimal amount of 0.9 μM could be detected, 2.5% of the total amount if every dye molecule produced an aniline molecule during the reaction. Initial thoughts were that the resultant aniline was subsequently adsorbed into the COP matrix, but further testing with dedicated sorption tests of aniline in aqueous solution with COP-1 and COP-19 could not prove that either are capable of adsorbing aniline. The combination of the observed patterns in the spectra and the detection of aniline conclude that, in addition to the dye decolourization due to adsorption, it is possible to degrade naphthol blue black; however, the primary benefit of these COPs appear to be first, stabilisation of nZVI in solution, and second, the adsorption of azo dyes and potentially an entire range of organic contaminants in the environment.

Ultimately, the main determining factors in the ability for the composite to remove the azo dye from solution were the BET surface area and the wettability of the base polymer. In general, the polymers with higher surface areas showed higher azo dye removal, the increased surface area and pore volume allowed for first adsorption and subsequent degradation once the dye had penetrated the polymer matrix. Even more significant is the water wettability, or ease of mixing into the dye containing water solution, of the root polymer. Although the exact solubility parameters have not yet been determined, COPs 1 and 19 exhibit strong hydrophilic properties due to the presence of polar groups, while COPs 6, 60, and 61 have exhibited quite hydrophobic properties. Possible reasons for the hydrophilicity most likely have to do with the presence of tertiary amine groups for COP-1 and the presence of unreacted aldehyde, secondary amine, and tertiary amine groups for COP-19; all of which can form hydrogen bonds and increase water solubility. Hydrophobicity of COP-6 is mainly due to the presence of

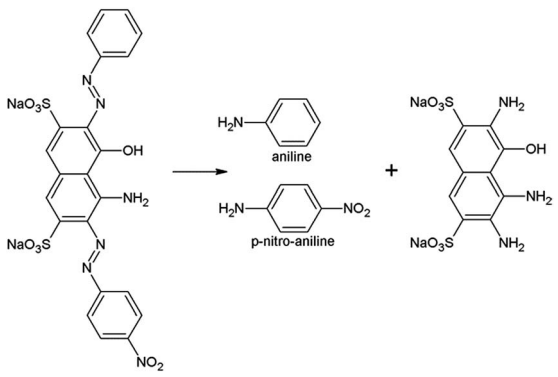


Scheme 1 Mechanism of the reductive degradation of naphthol blue black in the presence of nZVI.

Open Access Article. Published on 27 November 2015. Downloaded on 04/01/2016 06:14:04.
This article is licensed under a Creative Commons Attribution-NonCommercial 3.0 Unported Licence.

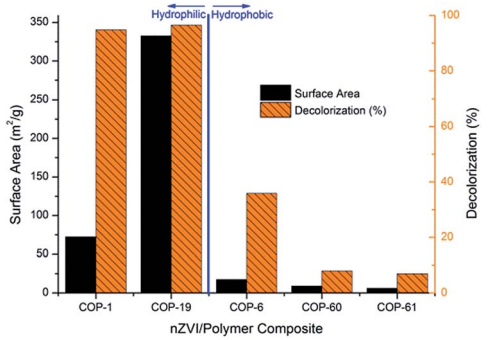


Fig. 6 Relationship of the composite surface area with decolourization ability towards naphthol blue black, in terms of removal percentage, organized by water affinity.

thioether groups and the aromaticity; COPs 60 and 61 also exhibit a high level of aromaticity; both of which make these compounds very insoluble in water. Wettability is a key factor, in that it allows for the contaminant to migrate into the composite material, where it can then be adsorbed, and further degraded by the impregnated nZVI.

The relationship of both the surface areas and the polymer wettability, with respect to decolourized naphthol blue black, is illustrated in Fig. 6.

## Conclusions

All five of the COPs utilized in this study, regardless of the BET surface area, pore volume, or wettability, were capable of successfully being impregnated with iron, at approximately equal loading rates. Although the morphologies varied widely from one COP to the other, ranging from thin sheath-like structures to globular clusters, iron was still observed to be contained within the various polymer matrices. The BET surface areas decreased in each polymer once the iron was impregnated, indicating that the pores were being filled. Each of the composites, especially COP-19, showed remarkable stability with respect to particle aggregation and sedimentation; vastly outperforming and remaining in suspension much longer, compared to commercially available products, which is a key parameter in the effectiveness of $Fe^0$ as a degrading agent. However, the composites of COPs 1 and 19 proved to be the most effective materials for decolourizing naphthol blue black, exhibiting high amounts of adsorption, and subsequent azo bond reduction as well as naphthalene group oxidation. This can be explained by both the high surface areas and the increased wettability of these two composites. Although, this phenomenon is more pronounced in the COP-1 composite, the COP-19 composite maintains too much adsorption to accurately determine degradation capacity. However, this combination adsorption/degradation provides a synergistic effect where large amounts of the contaminant can be drawn into and adsorbed within the composite matrix; then, subsequently providing an environment where the impregnated $Fe^0$ can degrade the contaminant. Construction of hydrophilic and high surface area COPs into larger aggregates with larger pore volumes would not only allow for more iron to be impregnated, but also allow for more contaminant diffusion into the composite matrix, providing a more suitable environment for contaminant degradation. These larger particles would then be ideal for immersion into a flow-through filter column designed for water treatment.

## Acknowledgements

P. D. M. and H. R. A. acknowledge funding for this study from the Technical University of Denmark (DTU) through the KAIST-DTU Signature Project on Integrated Water Technology. Y. H. acknowledges funding for this study through a DFF-Individual postdoctoral grant from the Danish Council for Independent Research – Technology and Production Science (4005-00393B). J. B. thanks the National Research Foundation of Korea (NRF) for a global Ph.D. fellowship (2013H1A2A1033423). J. B., H. A. P., and C. T. Y. acknowledge the financial support by Basic Science Research Program through the National Research Foundation of Korea (NRF), ICT & Future Planning (2013R1A1A1012998), and IWT (NRF-2012-C1AAA001-M1A2A2026588).

## References

1 R. Thiruvenkatachari, S. Vigneswaran and R. Naidu, *J. Ind. Eng. Chem.*, 2008, **14**, 145–156.
2 C.-B. Wang and W. Zhang, *Environ. Sci. Technol.*, 1997, **31**, 2154–2156.
3 R. A. Crane and T. B. Scott, *J. Hazard. Mater.*, 2012, **211–212**, 112–125.
4 J. Cao, L. Wei, Q. Huang, L. Wang and S. Han, *Chemosphere*, 1999, **38**, 565–571.
5 S. Nam and P. Tratnyek, *Water Res.*, 2000, **34**, 1837–1845.
6 T. Phenrat, N. Saleh, K. Sirk, R. D. Tilton and G. V. Lowry, *Environ. Sci. Technol.*, 2006, **41**, 284–290.
7 B. Schrick, B. W. Hydutsky, J. L. Blough and T. E. Mallouk, *Chem. Mater.*, 2004, **16**, 2187–2193.
8 F. He and D. Zhao, *Environ. Sci. Technol.*, 2005, **39**, 3314–3320.
9 T. Tosco, M. Petrangeli Papini, C. Cruz Viggi and R. Sethi, *J. Cleaner Prod.*, 2014, **77**, 10–21.
10 Y. Hwang, Y.-C. Lee, P. D. Mines, Y. S. Huh and H. R. Andersen, *Appl. Catal., B*, 2014, **147**, 748–755.
11 A. P. Côté, A. I. Benin, N. W. Ockwig, M. O'Keeffe, A. J. Matzger and O. M. Yaghi, *Science*, 2005, **310**, 1166–1170.
12 A. Thomas, *Angew. Chem., Int. Ed. Engl.*, 2010, **49**, 8328–8344.
13 Y. J. Choi, J. H. Choi, K. M. Choi and J. K. Kang, *J. Mater. Chem.*, 2011, **21**, 1073–1078.
14 B. M. Rambo and J. J. Lavigne, *Chem. Mater.*, 2007, **19**, 3732–3739.
15 W. Niu, C. O'Sullivan, B. M. Rambo, M. D. Smith and J. J. Lavigne, *Chem. Commun.*, 2005, 4342–4344.
16 L. M. Lanni, R. W. Tilford, M. Bharathy and J. J. Lavigne, *J. Am. Chem. Soc.*, 2011, **133**, 13975–13983.

 This journal is © The Royal Society of Chemistry 2016

Open Access Article. Published on 27 November 2015. Downloaded on 04/01/2016 06:14:04.
This article is licensed under a Creative Commons Attribution-NonCommercial 3.0 Unported Licence.

17 H. A. Patel, F. Karadas, A. Canlier, J. Park, E. Deniz, Y. Jung, M. Atilhan and C. T. Yavuz, *J. Mater. Chem.*, 2012, **22**, 8431–8437.
18 H. A. Patel, F. Karadas, J. Byun, J. Park, E. Deniz, A. Canlier, Y. Jung, M. Atilhan and C. T. Yavuz, *Adv. Funct. Mater.*, 2013, **23**, 2270–2276.
19 H. A. Patel, S. H. Je, J. Park, Y. Jung, A. Coskun and C. T. Yavuz, *Chem.–Eur. J.*, 2014, **20**, 772–780.
20 H. A. Patel, M. S. Yavuz and C. T. Yavuz, *RSC Adv.*, 2014, **4**, 24320–24323.
21 Y. Zhou, Z. Xiang, D. Cao and C.-J. Liu, *Chem. Commun.*, 2013, **49**, 5633–5635.
22 W. Wang, Z. Jin, T. Li, H. Zhang and S. Gao, *Chemosphere*, 2006, **65**, 1396–1404.
23 M. G. Schwab, B. Fassbender, H. W. Spiess, A. Thomas, X. Feng and K. Müllen, *J. Am. Chem. Soc.*, 2009, **131**, 7216–7217.
24 H. Kim, H.-J. Hong, J. Jung, S.-H. Kim and J.-W. Yang, *J. Hazard. Mater.*, 2010, **176**, 1038–1043.
25 C. T. Yavuz, J. T. Mayo, W. W. Yu, A. Prakash, J. C. Falkner, S. Yean, L. Cong, H. J. Shipley, A. Kan, M. Tomson, D. Natelson and V. L. Colvin, *Science*, 2006, **314**, 964–967.
26 D. D. Evanoff and G. Chumanov, *J. Phys. Chem. B*, 2004, **108**, 13957–13962.
27 L. L. Zawaideh and T. C. Zhang, *Water Sci. Technol.*, 1998, **38**, 107–115.
28 H.-Y. Shu, M.-C. Chang, H.-H. Yu and W.-H. Chen, *J. Colloid Interface Sci.*, 2007, **314**, 89–97.
29 S. Luo, P. Qin, J. Shao, L. Peng, Q. Zeng and J.-D. Gu, *Chem. Eng. J.*, 2013, **223**, 1–7.
30 K.-S. Wang, C.-L. Lin, M.-C. Wei, H.-H. Liang, H.-C. Li, C.-H. Chang, Y.-T. Fang and S.-H. Chang, *J. Hazard. Mater.*, 2010, **182**, 886–895.
31 A. Troupis, E. Gkika, T. Triantis, A. Hiskia and E. Papaconstantinou, *J. Photochem. Photobiol., A*, 2007, **188**, 272–278.
32 H. Zhu, Y. Jia, X. Wu and H. Wang, *J. Hazard. Mater.*, 2009, **172**, 1591–1596.
33 J. Byun, H. A. Patel, D. J. Kim, C. H. Jung, J. Y. Park, J. W. Choi and C. T. Yavuz, *J. Mater. Chem. A*, 2015, **3**, 15489–15497.
34 K. Yin, I. M. C. Lo, H. Dong, P. Rao and M. S. H. Mak, *J. Hazard. Mater.*, 2012, **227–228**, 118–125.
35 Y. Hwang, Y.-C. Lee, P. D. Mines, Y.-K. Oh, J. Seok Choi and H. R. Andersen, *Chem. Eng. Sci.*, 2014, **119**, 310–317.
36 N. Lee, K. Choi, B. Uthuppu, M. H. Jakobsen, Y. Hwang, M. M. Broholm and W. Lee, *Adv. Environ. Res.*, 2014, **3**, 107–116.
37 N. Saleh, K. Sirk, Y. Liu, T. Phenrat, B. Dufour, K. Matyjaszewski, R. D. Tilton and G. V. Lowry, *Environ. Eng. Sci.*, 2007, **24**, 45–57.
38 S.-H. Chang, S.-H. Chuang, H.-C. Li, H.-H. Liang and L.-C. Huang, *J. Hazard. Mater.*, 2009, **166**, 1279–1288.
39 C. Nasr, K. Vinodgopal, S. Hotchandani, A. K. Chattopadhyay and P. V. Kamat, *Res. Chem. Intermed.*, 1997, **23**, 219–231.
40 C. Nasr, K. Vinodgopal, L. Fisher, S. Hotchandani, A. K. Chattopadhyay and P. V. Kamat, *J. Phys. Chem.*, 1996, **100**, 8436–8442.